Protein Engineering vol.10 no.12 pp.1395–1405, 1997

Development of a structural model for the cytoplasmic domain of an integrin

Thomas A.Haas[1] and Edward F.Plow

Joseph J.Jacobs Center for Thrombosis and Vascular Biology, Department of Molecular Cardiology, Cleveland Clinic Foundation, 9500 Euclid Avenue, Cleveland, OH 44195, USA

[1]To whom correspondence should be addressed

The cytoplasmic tails of integrin heterodimers play central roles in controlling the activation states of integrins and in transmitting intracellular signals. Despite their short length, no structure of any integrin cytoplasmic domain has been determined. Therefore, molecular models for the cytoplasmic domain of $\alpha_{IIb}\beta_3$, the major platelet integrin, were generated, including models for the individual cytoplasmic tails, the binary α_{IIb}–calcium complex, and the ternary α_{IIb}–β_3–calcium complex. Structural analysis of circular dichroism spectra were compiled with data obtained from short homologous sequences within crystallized proteins, and with secondary structural predictions to develop starting models for each subunit. These models were subjected to a series of energy minimization and molecular dynamic simulations to generate final models. α_{IIb} was predicted to be ordered at its N-terminus and its C-terminus could accommodate a cation in a multicoordinated complex. The structure of β_3 was dominated by a β-turn at its NPXY motif ($\beta_3$744–747). In docking of α_{IIb} to different sites within β_3, the conformation of the β_3 juxta-transmembrane ($\beta_3$716–721) was greatly altered. This region was confirmed to be a conformational 'hot-spot' by circular dichroism. The conformational flexibility of this juxta-transmembrane region, which is highly conserved amongst integrins, is ideally located to regulate signaling.

Keywords: cytoplasmic domain/docking/integrin/juxta-transmembrane/molecular modeling

Introduction

Members of the integrin family of adhesion receptors recognize numerous extracellular ligands. Ligand occupancy of these receptors results in adhesive events which influence processes such as development, hemostasis, wound healing, inflammation, apoptosis and tumor metastasis (Hynes, 1992). Each subunit of an integrin α/β heterodimer contains a large extracellular region of several hundred amino acids, a transmembrane domain and usually a short cytoplasmic tail (Ruoslahti, 1991; Hynes, 1992; Ginsberg *et al.*, 1993). The extracellular regions of the integrin interact noncovalently to form a binding site(s) for a wide variety of ligands (Haas and Plow, 1994; Loftus *et al.*, 1994). High affinity ligand binding often involves activation of the integrin; i.e., cellular agonists initiate intracellular changes which ultimately render the extracellular domain competent to bind ligand. The process by which integrins modulate their affinity for their ligands is referred to as inside-out signaling (Ginsberg *et al.*, 1992; Hynes, 1992; Schwartz, 1992). Outside-in signaling denotes the activation of intracellular signaling pathways following ligand binding. A multitude of cellular responses, including protein phosphorylation, calcium mobilization, cytoskeleton assembly and reorganization, cell motility/spreading and gene expression are induced as a consequence of ligand occupancy of integrin receptors (Zhang *et al.*, 1992; Fox, 1993; Clark *et al.*, 1994; Clark and Brugge, 1995).

The integrin cytoplasmic tails are centrally involved in both outside-in and inside-out signaling, as they must either initiate or accept signals that are transmitted across the cell membrane. This premise is supported by data indicating that various cytoskeletal and signaling proteins can directly interact with the cytoplasmic tails of integrins (Horwitz *et al.*, 1986; Cappolino *et al.*, 1995; Clark and Brugge, 1995; Kieffer *et al.*, 1995; Law *et al.*, 1996). Indeed, several specific sequences within the cytoplasmic tails have been implicated in inside-out and outside-in integrin signaling. The α-actinin and talin binding sites in β_1 (Reszka *et al.*, 1992; Otey *et al.*, 1993), the calreteculin and F-actin binding site in α_2 (Rojiani *et al.*, 1993; Kieffer *et al.*, 1995), and the SHC and GRB2 in β_3 (Law *et al.*, 1996) have all been at least partially mapped. A naturally occurring serine to proline mutation, located in the cytoplasmic domain of β_3, $\beta_3$752, impairs both inside-out and outside-in signaling by $\alpha_{IIb}\beta_3$ (Chen *et al.*, 1992, 1994). Extensive mutational analyses also have provided further evidence that regions within both the α and β cytoplasmic tails play important roles in mediating bidirectional integrin signaling pathways (Marcantonio *et al.*, 1990; O'Toole *et al.*, 1991; Fornaro *et al.*, 1995; Hughes *et al.*, 1995; O'Toole *et al.*, 1995; Meredith *et al.*, 1995).

Despite the above cited advances in defining regions with the cytoplasmic tails which mediate integrin signaling, the structures of the α or β cytoplasmic tails remain essentially unknown. To address this problem, our laboratory has recently reported an initial structural analysis of the cytoplasmic domain of $\alpha_{IIb}\beta_3$ using synthetic peptides which encompass the entire intracellular region of the receptor (Haas and Plow, 1996). Summarizing our findings, the cytoplasmic tail of α_{IIb} was demonstrated to bind divalent cations with high affinity and to interact with the cytoplasmic tail of β_3, in the presence and absence of cations. These observations led us to conclude that the cytoplasmic domain of $\alpha_{IIb}\beta_3$ was a ternary complex composed of the cytoplasmic tails of α_{IIb}, β_3 and a divalent cation. In addition, the cation binding site and the inter-subunit interaction sites within both α_{IIb} and β_3 were mapped, and evidence was provided to suggest that a salt bridge may stabilize this ternary complex. These data were obtained using the synthetic peptide, and the occurrence of these interactions in the intact receptor, *in situ*, remains to be directly addressed. However, the existence of an inter-cytoplasmic tail salt bridge has independently been predicted by mutational analyses (Hughes *et al.*, 1996).

In the present study, we have expanded upon our previous study (Haas and Plow, 1996), and have developed molecular

models for the cytoplasmic tails of the α_{IIb} and β_3 subunits, for calcium bound to α_{IIb} and for the ternary $\alpha_{IIb}\beta_3$ cytoplasmic domain. These models have been built based upon primary biochemical data, homologies of small segments to known structures, and molecular dynamic simulations and energy minimizations. These models provide a framework for interpreting existing structure function data. In addition, the primary data and the models identify a region juxtapositioned to the transmembrane segment of the cytoplasmic domain of β_3 which is conformationally labile, and we propose that conformational changes in this region may be centrally involved in the transmission of outside-in and inside-out signaling.

Materials and methods

Materials

HPLC grade acetonitrile and methanol and peptide synthesis grade *N,N*-dimethylformamide were obtained from Fisher Scientific (Itasca, IL). NMR grade triflouroethanol (TFE), *p*-cresol and *p*-thiocresol were obtained from Aldrich (Milwaukee, WI). *tert*-butyloxycarbonyl (Boc)-Asp(OcHx) and Boc-Glu(OcHx) amino acids were from Novabiochem (La Jolla, CA). All other Boc-amino acids, as well as diisopropylethylamine, all peptide synthesis resins and TFA (for HPLC) were obtained from Advanced Chemtech (Louisville, KY). TFA used in peptide synthesis was obtained from Halocarbon (River Edge, NJ); 1-hydroxybenzotriazole tetramethyluronium hexafluoro-phosphate (HBTU) from Richelieu Biotechnologies (Montreal, QC); and ninhydrin reagents from Applied Biosystems (Foster City, CA).

Peptide synthesis

All peptides used in this study were synthesized using an automated and a manual stepwise *in situ* neutralization/HBTU protocol for Boc-chemistry solid phase peptide synthesis (Schnolzer *et al.*, 1993). The efficiency of coupling at each step was monitored using the quantitative ninhydrin method (Schnolzer *et al.*, 1993). Peptides were synthesized either on 4-methylbenzhydrylamine resins or on Boc-aminoacyl-OCH_2-Pam resins. Dinitrophenol, Boc and formyl protecting groups were removed prior to peptide cleavage. Full side chain deprotection and peptide cleavage from the resin was performed in liquid HF containing appropriate scavengers.

Peptide purification and characterization

All analytical and semipreparative gradient HPLC were performed on a Gilson 306 dual pump HPLC system equipped with a 811C dynamic mixer and a 117 dual wavelength detector (Gilson Inc., Middleton, WI). All HPLC runs were performed on Vydac C18 columns. Analytical runs were performed on a 5 μm, 4.6×250 mm column at a flow rate of 1 ml/min; and semi-preparative runs on a 10 μm, 22×250 mm column at a flow rate of 10 ml/min. Linear gradients of water:TFA (999:1) versus acetonitrile:water:TFA (900:99.1:0.9) were used in all HPLC runs.

Crude peptides were dissolved in 10% aqueous acetic acid, diluted 1:20 with 5% aqueous acetonitrile and 0.1% TFA, and purified by semi-preparative HPLC. Following lyophilization, the purity of each peptide was confirmed to be >98% as assessed by both analytical HPLC and electrospray ionization mass spectroscopy (Haas and Plow, 1996).

Peptide quantification and nomenclature

Peptide concentrations were determined by either tryptophan absorbance at 280 nm or 289 nm (ε = 5690 $M^{-1}cm^{-1}$ and 4850 $M^{-1}cm^{-1}$, respectively), tyrosine absorbance at 276 nm (ε = 1450 $M^{-1}cm^{-1}$), or by dry weight.

For peptide nomenclature, the subunit identification (α or β) is followed by the sequence position, with residue 1 being the N-terminus of the mature subunit (Fitzgerald *et al.*, 1987; Poncz *et al.*, 1987). Peptides containing a natural C-terminus were synthesized as carboxylates, otherwise peptide amides were synthesized. The peptides used in this study are as follows: α_{IIb}985–1008, LAMWKVGFFKRNRPPLEEDDEEGE; α-helix capped (HC) HC-α_{IIb}, GGSEDELAMWKVGFFKRNRPPLEEDDEEGE; α_{IIb}985–998, LAMWKVGFFKRNRP (amide); α_{IIb}999–1008, PLEEDDEEGE; $\beta_3$713–762, LIWKLLITIHDRKEFAKFEEERARAKWDTANNPLYKEATSTFTNITYRGT; $\beta_3$719–762, ITIHDRKEFAKFEEERARAKWDTANNPLYKEATSTFTNITYRGT; HC-β_3, GGSEDELIWKLLITIHDRKEFAKFEEERARAKWDTANNPLYKEATSTFTNITYRGT; and structural capped (SC) SC-β_3, SEDELIWKLLIATIHDRKEFAKFEEERARAKWDTANNPLYKEATSTFTNITYRGT.

Circular dichroism spectroscopy and secondary structural analysis

Circular dichroism (CD) spectra of the peptides were obtained as previously reported (Haas and Plow, 1996). Briefly, CD measurements were performed on a Jasco J600 spectropolarimeter equipped with a thermally regulated cell holder maintained at 4°C. Peptides were dissolved in 1 mM KCl, 5 mM phosphate, buffered to either pH 7.2 or 3.2 with KOH, and incubated for 30 min on ice. Samples were placed in a 2 mm rectangular quartz cuvette, and the region from 260 to 182 nm was scanned 5 times and an averaged spectrum obtained. The spectrum was then digitized, corrected for solvent contribution, converted into units of mean residual molar ellipticity (Θ, $deg.cm^2.dmol^{-1}$), exported into Peakfit (Scanalytics) and smoothed using a FFT transformation. Secondary structure was estimated as a linear combination of four secondary structural component spectra (α-helical, β-sheet, β-turn and random/extended coil) using 1 nm steps from 240 to 195 nm, as previously described (Haas and Plow, 1996).

Secondary structural predictions

Secondary structural predictions based on the primary sequences were performed using the Chou-Fasman and Gor II prediction methods as found in the Homology program [Molecular Simulations Inc. (MSI), San Diego].

Molecular modeling

Molecular dynamic simulations and model building were carried out using InsightII (MSI) using the program defaults, unless otherwise stated, on a Silicon Graphics Indigo workstation. The transmembrane/cytoplasmic boundaries for α_{IIb} and β_3 were predicted at the highly conserved α/β integrin lysine residue (K989 and K716 in α_{IIb} and β_3, respectively) using a transmembrane predictive analysis program (Rick *et al.*, 1995). These boundaries are in complete agreement with integrin mutational studies. Initial models of the cytoplasmic tails (which included a portion of the transmembrane region) of α_{IIb} and β_3 were constructed based on CD experiments, homology modeling, and secondary structural predictions (described in results section). The charges on the amino acids in each model were adjusted to pH 7.2. The cytosolic region of each cytoplasmic tail was then soaked with five layers of water and the minimized energy conformation obtained by gradually annealing the protein–water structure as previously

described (Bjornholm *et al.*, 1993). The resulting minimized structure was then subjected to a series of molecular dynamic simulations and energy minimizations, referred to as the molecular simulation procedure. A typical molecular simulation procedure was performed as follows: 10 000 steps of molecular dynamic simulations were performed using a time step of 1 fs, a van der Waals cut off of 12 Å an electrostatic cut off of 19 Å, and using the group-based summation method. The resulting structure was then minimized to a maximum derivative of less than 5 kcal·(mol·Å)$^{-1}$ using the steepest descent minimization algorithm, and then to less than 1 kcal·(mol·Å)$^{-1}$ using conjugate gradient minimization. The structure was then subjected to 10 cycles of the above dynamics/minimization procedure, saving the structure obtained after each cycle. After the cycling procedure, the van der Waals and electrostatic cut offs were removed and a final energy-minimized structure was obtained with a maximum derivative of less than 0.001 kcal·(mol·Å)$^{-1}$ using conjugate gradient minimization.

To generate models of the binary α_{IIb}–calcium complex, a molecular simulation procedure, similar to the one described by Tuckwell *et al.* (1993), was followed. Briefly, calcium was docked to α_{IIb}, the structure soaked in water and the assembly minimized to a deviation of <1 kcal·(mol·Å)$^{-1}$. The assembly was then subjected to 500 fs of molecular dynamics at 295 $\pm$ 5 K. The temperature was increased by 5 K and the dynamic simulations repeated until a final temperature of 320 K was reached. At 320 K, molecular dynamics was performed for 50 ps, and then the temperature was cooled down to 295 K by reversing the heating procedure. The temperature was then adjusted to 298 K, and the molecular simulation procedure used to generate Model α_{IIb} was followed; i.e., all α_{IIb}–calcium models were subjected to >160 ps of molecular dynamic simulations.

Dockings were performed manually with a distance cut off of 15 Å using MSI's Docking program. Final van der Waals and electrostatic energies of interaction were obtained using a distance cut off of 100 Å. When present, the transmembrane domains of α_{IIb} and β_3 were left in vacuum.

Results

Cytoplasmic tail of α_{IIb}

Conformation of α_{IIb}. The conformation of a synthetic peptide encompassing the cytoplasmic tails of α_{IIb} was examined by CD spectroscopy (Figure 1). The CD spectrum of α_{IIb}985–1008 in aqueous solution at 4°C (Figure 1A) exhibited a single minimum at 203 nm, a characteristic of peptide in a random coil. Aqueous TFE solutions are presumed to mimic a phospholipid bilayer environment and to stabilize the conformational propensities of peptides (Buck *et al.*, 1993; Sticht *et al.*, 1994; Yang *et al.*, 1994; Chuang *et al.*, 1996). Addition of 50% TFE to α_{IIb}985–1008 altered its CD spectrum; the minimum was shifted to 208 nm and an additional negative peak appeared at 222 nm. These changes are indicative of acquisition of α-helical structure. Least-squared regression analysis was used to estimate the secondary structure of the peptide from the CD spectra. The helical content of the peptide increased from 5.2% in 0% TFE to 12.1% in 50% TFE, with a concomitant decrease in random coil from 32.2% to 27.1%. Less than 1% content of β structure, either β-sheet or β-turn, was estimated in the presence or absence of TFE. Only the α-helical structure of α_{IIb}985–1008 was stabilized using different solvent conditions: other concentrations of TFE (5, 10, 20, 30 and 40%), or low pH (3.0 and 4.5) (data not shown).

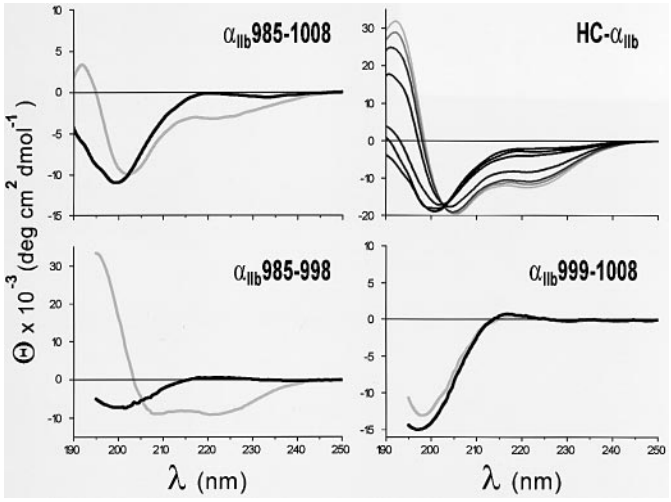

Fig. 1. The CD spectra of various α_{IIb} peptides (α_{IIb}985–1008, α_{IIb}985–998 and α_{IIb}999–1008) were obtained in 5 mM phosphate, pH 7.2, in the absence (black line) or presence of 50% TFE (grey line). The CD spectra for HC-α_{IIb} was obtained in the presence of increasing amounts of TFE (0, 5, 10, 20, 30, 40 and 50% TFE), with the percentage of TFE indicated by the darkness of the lines (darkest line = 0% TFE, and the lightest line = 50% TFE). All CD spectra were obtained at peptide concentration of 30 μM, and were performed at either 20°C (α_{IIb}985–1008 and HC-α_{IIb}) or 4°C (α_{IIb}985–998, and α_{IIb}999–1008).

The α-helical content of α_{IIb}985–1008 was also stabilized by the addition of an α-helix capping sequence, GGSEDE, to its N-terminus (HC-α_{IIb}; Figure 1). The addition of these residues have been shown to induce helical structure in a number of model peptides (Lyu *et al.*, 1992; Lyu and Wemmer, 1993) and also would mimic the effect of an α-helix in the transmembrane region. The α-helical content of HC-α_{IIb} in 0% TFE was equivalent to that observed with uncapped α_{IIb}985–1008 in 50% TFE (12.6 versus 12.1%, respectively). Addition of 50% TFE further increased the helical content of the capped peptide to 59.7%.

The α_{IIb}985–1008 sequence, LAMWKVGFFKRNRPPLEEDDEEGE, can be divided by the proline–proline at α_{IIb}998–999 into a hydrophobic/positively charged terminal aspect (α_{IIb}985–997) and an acidic terminus (α_{IIb}1000–1008). Peptides corresponding to these segments were synthesized to determine which region within α_{IIb}985–1008 gave rise to its helical potential. The CD spectra of peptides encompassing these two peptides, α_{IIb}985–998 and α_{IIb}999–1008, are displayed in Figure 1C and D, respectively. The helical content of α_{IIb}985–998 was 10.6% in buffer and increase to 15.0% upon the addition of TFE. Interestingly, 50% TFE also dramatically increased the β-sheet content of α_{IIb}985–998 (from <0.1% in 0% TFE to 47.2% in 50% TFE). This result was not observed with full-length α_{IIb}985–1008 at any TFE concentration tested. α_{IIb}999–1008 showed no propensity to assume an organized structure. Its content of α-helix was low, ~4%, and its calculated random coil content was high, ~40%. Changes in ionic strength, pH, temperature, organic solvent content and the addition of divalent cations all failed to alter the structure of α_{IIb}999–1008. Taken together, these results demonstrate that α_{IIb}985–1008 is capable of acquiring helical structure; this structure could be induced either by TFE or by a helical cap; and most of the helical potential of α_{IIb}985–1008 resides in its terminal region.

Table I. Secondary structural predictions for the integrin α cytoplasmic tails

Subunit	Sequence	PM[a]
α_{IIb}	LLLTILVLAMWKVGFFKRNRPPLEEDEEGE	
	hhhhhhhsssssstttt	CF
	sssshhhhhhhhhhhhttcctctthhhhhh	GorII
α_v	LLLAVLVFVMYRMGFFKRVRPPQEEQEREQLQPHENGEGNSET	
	sssssssssssssss tttt	CF
	hhhhhhhhhhhhhhhhhtcccttthhhhhhhhctttttttccctt	GorII
α_1	LLLMLLILALWKIGFFKRPLKKKMEK	
	hhhhhhhhhhssss	CF
	hhhhhhhhhhhhhhhhhhhhhhhhh	GorII
α_2	LLLLALVAILWKLGFFKRKYEKMTKNPDEIDETTELSS	
	sssssssssssssss tttt	CF
	hhhhhhhhhhhhhhhhhhhhhthccccthhhhhhhht	GorII
α_3	LLLGLIILLLWKCGFFKRARTRALYEAKRQKAEMKSQPSETERLTDDY	
	sssssssssssssss	CF
	sssssssshhhhhhhhhhhhhhhhhhhhhhhhhhhhtctttthhssttt	GorII
α_4	IVLLLISYVLWKAGFFKRQYKSILQEENRRDSWSYINSKSNDD	
	sssssssss sssssssssss ttttsssttt	CF
	sssssssshhhhhhhhhhhttthhhhhhhhttsssttcccct	GorII
α_5	LLLGLLIYILYKLGFFKRSLPYGTAMEKAQLKPPATSDA	
	sssssssssssssss tttt hhhhhh tttt	CF
	hhttsssshhhhhthssttctttchhhhhhtcccccct	GorII
α_6	LMLALLVFILWKCGFFKRNKKDHYDATYHKAEIHAQPSDKERLTSDA	
	hhhhhsssssssssss tttt sss tttt	CF
	hhhhhhhhhhhhhhhhhhhttttthhhhhhhhhhhhctttthhhssstth	GorII

Secondary structural predictions were performed using either the Chou-Fasman (CF) or the Gor II (GorII) prediction methods. Sequences predicted to be in an α-helical (h), β-sheet (s), βb-turn (t) or a random coil (c) conformation are indicated.
[a]Prediction method.

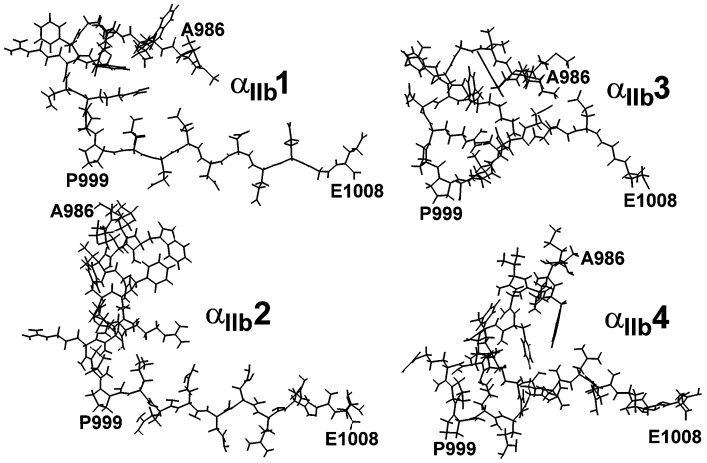

Fig. 2. Molecular models of α_{IIb}. The final eneregy minimized structures of Model α_{IIb}1–4 are displayed. For clarity, only the backbone of each structure of α_{IIb}984–1008 is displayed. For orientation, the relative positions of α_{IIb}A986, α_{IIb}P999 and α_{IIb}E1008 are indicated in all four models.

Molecular model of the cytoplasmic tail of α_{IIb}

A homology search of the Brookhaven Protein Data Base using the FASTA program (MSI) revealed no homologous protein sequences for the cytoplasmic tail of α_{IIb}, using α_{IIb}960–1008 as the target sequence. Using shorter target sequences of nine amino acids, five protein sequences homologous to α_{IIb}1000–1008 were identified, but these failed to adopt a consensus conformation. As a second strategy, the secondary structure of the cytoplasmic tail was predicted. The Chou-Fasman and Gor II methods were applied to α_{IIb}986–1008 as well as to several integrin α cytoplasmic tails (Table I). The two methods yielded a major and consistent difference in the structure predicted for α_{IIb}989–995 (KVGFFKR), and as for this highly conserved region within all eight α subunits analyzed: a β-sheet conformation was always predicted for this region using the Chou-Fasman method, and the Gor II method always predicted an α-helical conformation (Table I). As noted above, this dichotomy was reflected in the CD spectra: the shorter α_{IIb}985–998 peptide could adopt significant β structure, whereas the longer α_{IIb}996–1008 always assumed an α-helical conformation (Figure 1).

With the failure of the above approaches to develop a consensus starting conformation for α_{IIb}986–1008, two models were chosen as starting points for our molecular dynamic simulations and energy minimizations (Figure 2). In the first (model α_{IIb}1), α_{IIb}986–995 initially was assigned a right-handed α-helical conformation and the remaining amino acids were left in the extended conformation. In the second model (model α_{IIb}2), the helix was further shortened, terminating at α_{IIb}991. The peptide structure of each model was soaked in water, the energy of the assembly (peptide + water) was minimized, and then each model was then subjected to the molecular simulation procedure, resulting in an intermediate structure for model α_{IIb}1 and model α_{IIb}2. The molecular simulation procedure was then repeated on these structures to generate model α_{IIb}3 from model α_{IIb}1 and model α_{IIb}4 from model α_{IIb}2 (Figure 2). Deviations in the structures of all four models were identified by superimposition of their backbones. Model α_{IIb}3 was found to be the most similar to all the other models (r.m.s. deviations of alignment of 4.71, 5.62 and 4.77). Most importantly, α_{IIb}990–997, the region of dubious conformation, achieved almost identical conformations in all models (r.m.s. deviations of alignment of 1.49, 1.71 and 1.44).

Model α_{IIb}3 was then used as a starting template in constructing a final model of α_{IIb} which included a few amino acids of the extracellular domain and the entire transmembrane region as well as cytoplasmic domain (model α_{IIb}, Figure 3). The additional amino acids, α_{IIb}960–962 and α_{IIb}963–987, were assigned an extended and an α-helical conformation, respectively. Separate predictive analysis using the program of Riek (1995), supported the supposition that the transmembrane segment would conform to an α-helix. The extracellular and cytoplasmic regions of α_{IIb} were soaked in water, the assembly minimized, 10 ps of the molecular dynamics performed, and then the molecular simulation procedure was performed in 10 ps cycles, using a time step of 1 fs, for a total of 100 ps. The minimized structures obtained after every 10 ps cycle (cycle structures) and the final minimized structure of α_{IIb} (model α_{IIb}) are displayed (Figure 3A and B, respectively). Superimposition of the 10 cycle structures of α_{IIb}960–1008 revealed very little deviation in backbone structure (Figure 3A), indicating that a local minimum energy structure for α_{IIb}960–1008 was achieved. Common to all cycle structures and to model α_{IIb} was the formation of a loop region at α_{IIb}966–1001, while α_{IIb}1002–1008 remained in a random coil/extended conformation. Several side-chain and backbone interactions within α_{IIb}995–1003 were observed (Figure 3B), which presumably help to stabilize the conformation of the cytoplasmic tail of α_{IIb}

Docking of calcium to the cytoplasmic tail of α_{IIb}

Our previous study demonstrated that terminal α_{IIb}999–1008 region contained a high affinity cation binding site (Haas and Plow, 1996) and, therefore, models with calcium bound to the

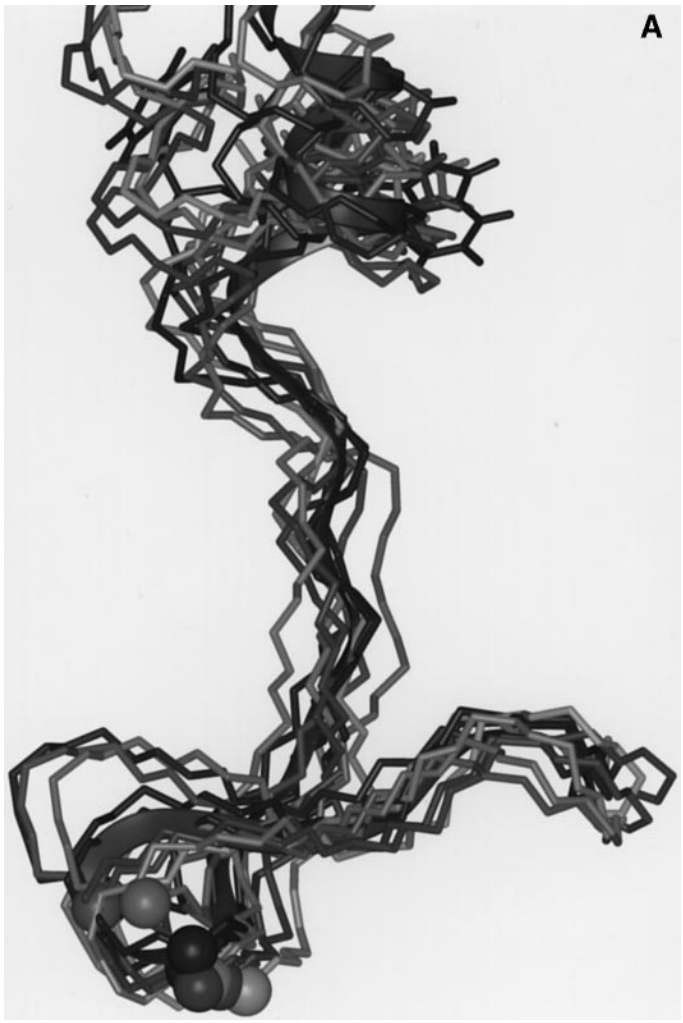

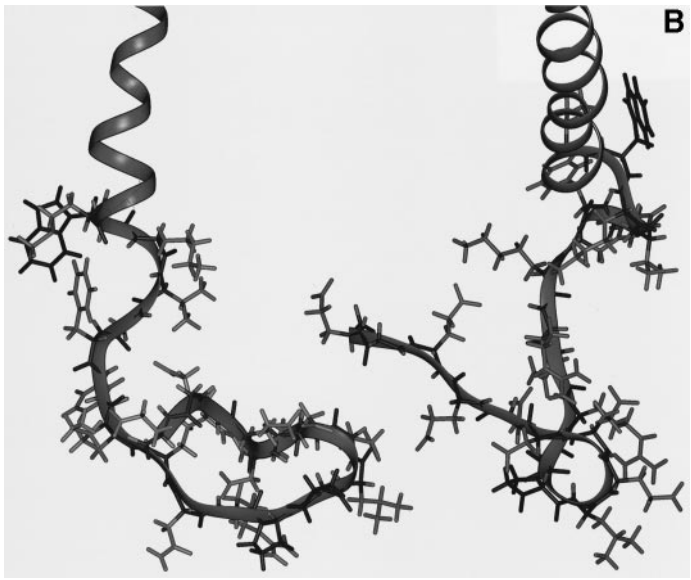

Fig. 3. Molecular dynamic models of α_{IIb}. The 10 energy minimized structures (**A**) obtained during the molecular simulation procedure and the final energy minimized structure (**B**) of model α_{IIb} are displayed. (A) For clarity, only the backbone of each structure of α_{IIb}984–1008 is displayed, and the backbone of the fifth structure is highlighted with a ribbon. For orientation, the Cα′s of prolines α_{IIb}998 are displayed as a sphere, and the side chain of tryptophan α_{IIb}989 (structure 5) is displayed. Note that there is very little deviation in the structure of α_{IIb}992–1008, while considerable variation is observed at α_{IIb}984–990. (B) The backbone and side chains of α_{IIb}989–1008 are displayed. The backbone is highlighted with a ribbon, and the side chain of tryptophan α_{IIb}989 is darkened for orientation. Two views of the model are displayed. The model on the left is the structure obtained as viewed perpendicular to the axis of the transmembrane domain, while the one on the right is viewed from about 20° off of the transmembrane axis, looking down from the extracellular domain, toward the cytoplasmic region.

cytoplasmic tail of α_{IIb} were developed. With the structure of α_{IIb} fixed, as displayed in Figure 3, calcium could be docked to three areas of local minimal energy within α_{IIb}999–1008. As all three sites of cation α_{IIb} interaction seemed feasible based upon biochemical data, models for all three interactions were generated using a molecular dynamic simulation procedure (see Materials and methods), similar to one used to confirm the affinity site of putative extracellular integrin calcium binding domains (Tuckwell *et al.*, 1993).

The final minimized structures for the α_{IIb} in all three models (model α_{IIb}:Cal-3) retained a tightly bound calcium ion (Figure 4). A similar molecular dynamics procedure resulted in the loss of calcium to an extracellular integrin cation binding domain of low affinity but not to one of high affinity (Tuckwell *et al.*, 1993), indicating that calcium was bound to α_{IIb} with high affinity in each of our models. This conclusion is in agreement with the apparent high affinity of this cation binding site relative to the extracellular cation sites of $\alpha_{IIb}\beta_3$ (Haas and Plow, 1996). In all three models, at least four cation coordination sites were identified (Table II), two of which were provided by one of the aspartate side chains (OD1 or OD2) of α_{IIb}1003–1004. These results are in complete agreement with variant α_{IIb} peptides (Haas and Plow, 1996), in which replacement of the two aspartic acids at α_{IIb}1003–1004 with alanines destroyed the divalent cation binding capacity of the resulting peptide. In further support of these

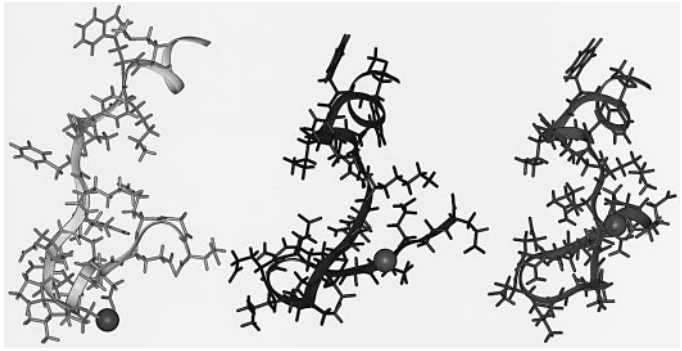

Fig. 4. Molecular models of the α_{IIb}:cation complex. The three models of the cytoplasmic tail of α_{IIb} containing a bound cation (α_{IIb}:Ca1–3) are displayed from left to right, respectively. The backbone of each model is highlighted with a ribbon and the calcium ion is displayed as a sphere. The N-terminus of each peptide is at that top and the C-terminus points to the right.

models, substitution of glutamic acid α_{IIb}1008 with alanine did not affect cation binding, and this carboxylated side chain was not used to coordinate calcium in any of the three models. However, since the terminus of α_{IIb} was found not to coordinate cation binding (Haas and Plow, 1996), model α_{IIb}:Ca3, in which the calcium was coordinated by the C-terminus (Table II, E1008:OXT) seems less likely.

Table II. Coordination sites of calcium binding to α_{IIb}

Model no.	Coordinating site[a]	Distance (Å)
α_{IIb}:Ca1	D1103:OD1	2.39
	D1003:OD2	2.39
	P999:O	2.66
	L1000:O	2.68
α_{IIb}:Ca2	D1004:OD2	2.34
	R995:O	2.49
	D1004:OD1	2.51
	E1006:O	2.59
α_{IIb}:Ca3	D1004:OD2	2.33
	E1008:OXT	2.36
	R995:O	2.43
	E1008:O	2.45
	D1004:OD1	2.56
	G1007:O	2.60

Atoms within α_{IIb} which were identified as putatively cation coordination sites in the various models are shown. Only atoms with a distance of less than 3 Å away from calcium are displayed and all water molecules were excluded.

[a]Nomenclature used: single letter code, sequence number and coordinating atom.

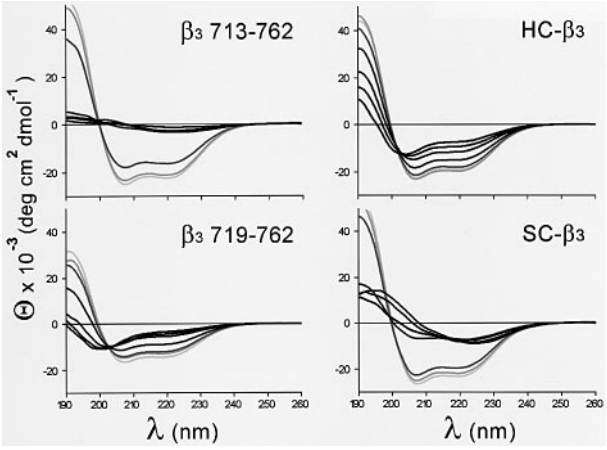

Fig. 5. Circular dichroism spectra of β_3 peptides. Various β_3 peptides (30 μM) were dissolved in 5 mM phosphate, containing increasing amounts of TFE (0 to 50% TFE). The percentage of TFE present in each sample is indicated by the darkness of the lines, with the darkest line indicating the CD spectra obtained at 0% TFE and the lightest line indicating the results obtained at 50% TFE. All CD spectra were obtained at 20°C.

Cytoplasmic tail of β_3

Conformation of the β_3 cytoplasmic peptide. The CD spectra of the β_3 cytoplasmic tail (Figure 5) were considerably more complicated than those of α_{IIb}. In 5 mM phosphate buffer, pH 7.2, the percentages of secondary conformation present in $\beta_3$719–762 were 8.0% α-helical, 18.2% β-sheet, 3.2% β-turn and 49.9% random coil (Figure 5, lower left panel). The addition of TFE resulted in a concentration dependent increase in α-helical content (33.7% α-helical at 50% TFE), coinciding with a decrease in β-sheet (5.6%) and random coil (19.0%) content. Thus, only the α-helical structure of $\beta_3$719–762 was stabilized by TFE. However, extending the N-terminus of $\beta_3$719–762 by only six amino acids, $\beta_3$713–762, generated a peptide with dramatically different conformational characteristics (Figure 5). At 0% TFE, $\beta_3$713–762 had little structure (7.3% β-sheet, 3.4% random coil, <1% α-helix and <1% β-turn content); but addition of only 5% TFE increased its β-sheet content to 16.0%. At 20% TFE, the β-sheet content of $\beta_3$713–762 remained elevated (15.3%) and the helical content was low (2.2%). However, above 20% TFE the peptide acquired extensive helical structure, reaching a maximal helicity of 46.2% (7.2% β-sheet, <1% of β-turn, 20.9% random coil) in 50% TFE. This switch in conformation from a β-sheet to an α-helical peptide was either exaggerated or suppressed by the addition of conformational peptide caps to the N-terminus of $\beta_3$713–762 (Figure 5, right panels). In the absence of TFE, addition of an α-helix cap (GGSEDE) to $\beta_3$713–762 (HC-β_3) stabilized both the α-helical (16.2%) and β-sheet (13.1%) properties. Unlike $\beta_3$713–762, low TFE concentrations did not stabilize β-sheet content, but rather stabilized the α-helical content of HC-β_3. In contrast, addition of the SEDE structural to β_3 (SC-β_3, Figure 5), exaggerated the capacity of SC-β_3 to form a β-sheet (31.0 and 45.6% β-sheet for SC-β_3 in 0 and 10% TFE, respectively). Taken together, these data indicate that the β_3 cytoplasmic tail is conformationally labile and that the capacity to transit between β-sheet and α-helix must be located near and/or within $\beta_3$716–721. Finally, all three peptides ($\beta_3$713–762, HC-β_3 and SC-β_3) exhibited nearly identical secondary conformations at high percentages of TFE (40–50%). Thus, TFE stabilized peptide conformation at a high concentration but accentuated the conformational lability of the β_3 peptides at low concentrations.

Molecular model of the β_3 cytoplasmic tail

An initial model of the β_3 cytoplasmic tail was developed by compiling structural data from a number of sources. A homology search of the Brookhaven Protein Data Base yielded several proteins of known structures containing only short homologous regions to the cytoplasmic tail of β_3 (lactoferrin, neuramidase, glutathione *S*-transferase, β-galactose/glucose binding protein, β-lactmase and TPA kringle 2 domain). NMR studies have identified that NPXY sequences within several receptors, such as the LDL receptor and the insulin receptor, adopt a type 1 β-turn conformation (Bansal and Gierasch, 1991; Backer *et al.*, 1992). All β integrin subunits contain a NPLY sequence, including $\beta_3$744–747. Finally, as the integrin β subunits of are very homologous, a consensus secondary structural prediction of the β subunits was constructed. For certain segments, there was concurrence between the Gor II and Chou-Fasman methods (Table III), and their assigned conformations were in agreement with the crystal structure of proteins with homologous sequences.

Based upon these data, $\beta_3$744–747 (type 1 β-turn), $\beta_3$710–716 and $\beta_3$723–738 (right handed α-helix) and $\beta_3$752–756 (β-sheet) were all initially assigned conformations. However, the conformation of $\beta_3$717–722 was inconsistent among the various analyses so that three separate models served as starting points. In the first model, model $\beta_3$1, the α-helix of $\beta_3$710–716 was extended through $\beta_3$738. In the second model, model $\beta_3$2, the α-helix of $\beta_3$710–716 was extended only to $\beta_3$718, and in the third model, model $\beta_3$3, $\beta_3$718–721 was placed in a β-sheet conformation. All models were then soaked (from $\beta_3$716–762), and the assembly was minimized. Fifty ps of molecular dynamics, followed by 100 ps of molecular simulation procedure were then performed, resulting in three final structures. Three addition models (model $\beta_3$4–6, respectively) were generated by removing the water from the starting minimized assemblies and repeating the same molecular simulation procedures using a dielectric constant of 80. These later three models were generated to confirm that the water–vacuum interface near the transmembrane segment did not substantially

Table III. Secondary structural predictions for the integrin β cytoplasmic tails

Subunit	Sequence	PM[a]
β_3	LIGLAALLIWKLLITIHDRKEFAKFEEERARAKWDTANNPLYKEATSTFTNITYRGT	
	hhhhhhhhhhssssss hhhhhh tttt sssssssssttt	CF
	hhhhhhhhhhhhhhhhhhhhhhhhhhhhhhhhhhhhhhtttcchhhttsssssssssstc	GorII
β_1	LIGLALLLIWKLLMIIHDRREFAKFEKEKMNAKYNTGENPIYKSAVTTVVNPKYEGK	
	sssssssssssssssss ttttsssssssssssttttt	CF
	sshhhhhhhhhhhhhhhhhhhhhhhhhhhhhhhhhhttttccssssssssssscccctttt	GorII
β_{1M}	LIGLALLLIWKLLMIIHDRREFAKFEKEKMNAKWDTGENPIYKSAVTTVVNPKYEGK	
	sssssssssssssssss ttttsssssssssssttttt	CF
	sshhhhhhhhhhhhhhhhhhhhhhhhhhhhhhhhhhhttttcchsssssssssscccctttt	GorII
β_2	LIGILLLVIWKALIHLSDLREYRRFEKEKLKSQWN-NDNPLFKSATTTVMNPKFAES	
	sssssssssssssssss ttttsssssssshhhhhh	CF
	ssssshhhhhhhhhhhhhhhhhhhhhhhhhhhttt ttcchhsstcsssccctthhhh	GorII
β_{2M}	LIGVLLLVIWKALTHLTDLREYRRFEKEKLKSQWN-NDNPLFKSATTTVMNPKFAES	
	sssssssssssssssss ttttsssssssshhhhhh	CF
	sssssshhhhhhthhhhhhhhhhhhhhhhhhttt ttcchhsstcsssccctthhh	GorII
β_5	LVGLALLAIWKLLVTIHDRREFAKFQSERSRARYEMASNPLYRKPISTHTVDFTFNKSY[b]	
	hhhhhhhhhhhssssss hhhhhh sttttsssssssssssstttt	CF
	sshhhhhhhhhhshhhhhhhhhhhhhhhhhhhhhhhhttccttttctscsssssssstttt	GorII
β_{5M}	LIGLALLLIWKLLMIIHDRREFAKFEKEKMNAKWDTGENPIYKSAVTTVVNPKYEGK	
	sssssssssssssssss ttttsssssssssssttttt	CF
	sshhhhhhhhhhhhhhhhhhhhhhhhhhhhhhhhhhhttttcchsssssssssscccctttt	GorII
β_6	LIGVVLLCIWKLLVSFHDRKEVAKFEAERSKAKWQTGTNPLYRGSTSTFKNVTYKHREK[c]	
	sssssssssssssssss hhhhhhssssss sssssssssssssssss	CF
	sssssssshhhhhhhhhhhhhhhhhhhhhhhhhhhhsttcccsssstcssssstthhhhhhhh	GorII

Secondary structural predictions were performed using either the Chou-Fasman (CF) method or the Gor II (GorII) method. Sequences predicted to be in an α-helical (h), β-sheet (s), β-turn (t) or a random coil (c) conformation are indicated.
[a]Prediction method;
[b]continuation of β_5 sequence: NGTVD;
[c]continuation of β_6 sequence: QKVDLSTDC.

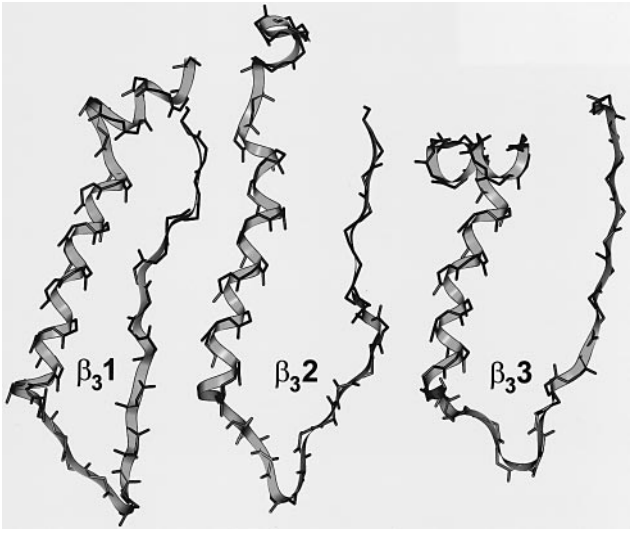

Fig. 6. Molecular models of β_3. The final energy minimized structures of Model $\beta_3$1–3 are displayed. Only the backbone of $\beta_3$711–762 are displayed, which is highlighted with a ribbon. The C-terminus of β_3 in all three models is on the right, and the NPXY turn motif, $\beta_3$744–747, is at the bottom apex of models. The structures of the helical region ($\beta_3$723–737) and the NPXY turn motif are conserved in all three models.

affect the final structures obtain for $\beta_3$717–722. Thus, three types of models were generated based on the starting structure of $\beta_3$717–722: a helical model (model $\beta_3$1 and $\beta_3$4), an extended model (model $\beta_3$2 and $\beta_3$5) and a β-sheet model (model $\beta_3$3 and $\beta_3$6).

The structures obtained from the three assembly models of β_3, model $\beta_3$1–3, are displayed in Figure 6. Superimposition of the backbone of model $\beta_3$1 onto models $\beta_3$2 and $\beta_3$3, revealed that the helical structure of $\beta_3$723–735 (r.m.s. deviations of alignment of 1.14 and 0.95), and the β-turn (r.m.s. deviations of alignment of $\beta_3$740–748 were 1.66 and 1.08) were conserved, while the conformation of $\beta_3$717–721 converged towards one structural conformation (r.m.s. deviations of 1.77 and 1.36). It also appeared that the turn motif at $\beta_3$744–747 was stabilized by the formation of a salt bridge between the aspartic acid at $\beta_3$740 and the lysine at $\beta_3$748. Furthermore, the structure of $\beta_3$717–721 was not affected to any great extent by the water vacuum interface, as similar structures were obtained for this region in the absence of water (r.m.s. deviations of 1.14, 0.26 and 0.23 of water versus non-water models). Thus, of the three types of models generated, the helical model of β_3 underwent the greatest conformational change in structure for $\beta_3$717–721, merging towards a common structural conformation.

Model $\beta_3$1 was chosen as the starting point to construct a model of β_3 encompassing its entire transmembrane/cytoplasmic domain ($\beta_3$682–762), model β_3. In model β_3, the additional amino acids were initially assigned either an extended conformation ($\beta_3$682–690) or a right-handed α-helical conformation ($\beta_3$691–715). The extracellular ($\beta_3$682–691) and cytoplasmic ($\beta_3$716–762) domains were soaked with water and the assembly was minimized. The assembly was then subjected to 50 ps of molecular dynamics, followed by 100 ps of molecular simulation procedure. The minimized structures obtained after each 10 ps cycle of the molecular simulation procedure (Figure 7A), and the final minimized structure of Model β_3 are displayed (Figure 7B).

As shown in Figure 7A, very little deviation in the structure of the backbone at $\beta_3$723–737 was observed. The backbone of $\beta_3$740–748, which encompassed the NPXY turn motif ($\beta_3$744–747), also deviated very little, but the relative alignment of the axis of this backbone to the rest of β_3 varied considerably. Considerable variation in structure was observed for $\beta_3$704–717, initiated by the flexibility of the glycine residue at $\beta_3$708, which destabilized the transmembrane α-helix of β_3. Similar α-helix destabilization by glycine $\beta_3$708 was observed in numerous models of the transmembrane domain of β_3 (data not shown). Similar to the initial six models for the cytoplasmic domain of β_3 (model $\beta_3$1–6), $\beta_3$723–735 (α-helical) and $\beta_3$744–747 (β-turn) retained their predicted structures, and the salt bridge between $\beta_3$740 and $\beta_3$748 was maintained (Figure 7B). Other possible intra-subunit contacts sites which may play important roles in stabilizing the structure of the cytoplasmic domain of β_3 are highlighted in Figure 7B. These include other possible salt bridges, β_3R736–β_3E749 and β_3R736–β_3D740, as well as several hydrophobic interactions.

Modeling the cytoplasmic ternary complex of $\alpha_{IIb}\beta_3$

Our previous study (Haas and Plow, 1996) and that of Hughes *et al.* (1996), indicated that inter-subunit salt bridges between the two cytoplasmic tails of $\alpha_{IIb}\beta_3$ may be responsible for maintaining cytoplasmic domain of $\alpha_{IIb}\beta_3$ in a complex, α_{IIb}999–1008 interacted with $\beta_3$721–740 in the presence of a divalent cation (Haas and Plow, 1996), the salt bridge was predicted between arginine α_{IIb}995 and aspartate α_{IIb}723 (Hughes *et al.*, 1996). Both of these data sets were taken into consideration separately to create two docking models for the subunit complex. In both models, a ternary calcium–α_{IIb}–β_3 cytoplasmic complex was generated by docking the α_{IIb}–calcium complex (model α_{IIb}–Ca2) with β_3 (model β_3), after removal of the water from both assemblies. In the first model, model $\alpha_{IIb}\beta_3$Ca1, α_{IIb}999–1008 was docked to $\beta_3$721–740, and

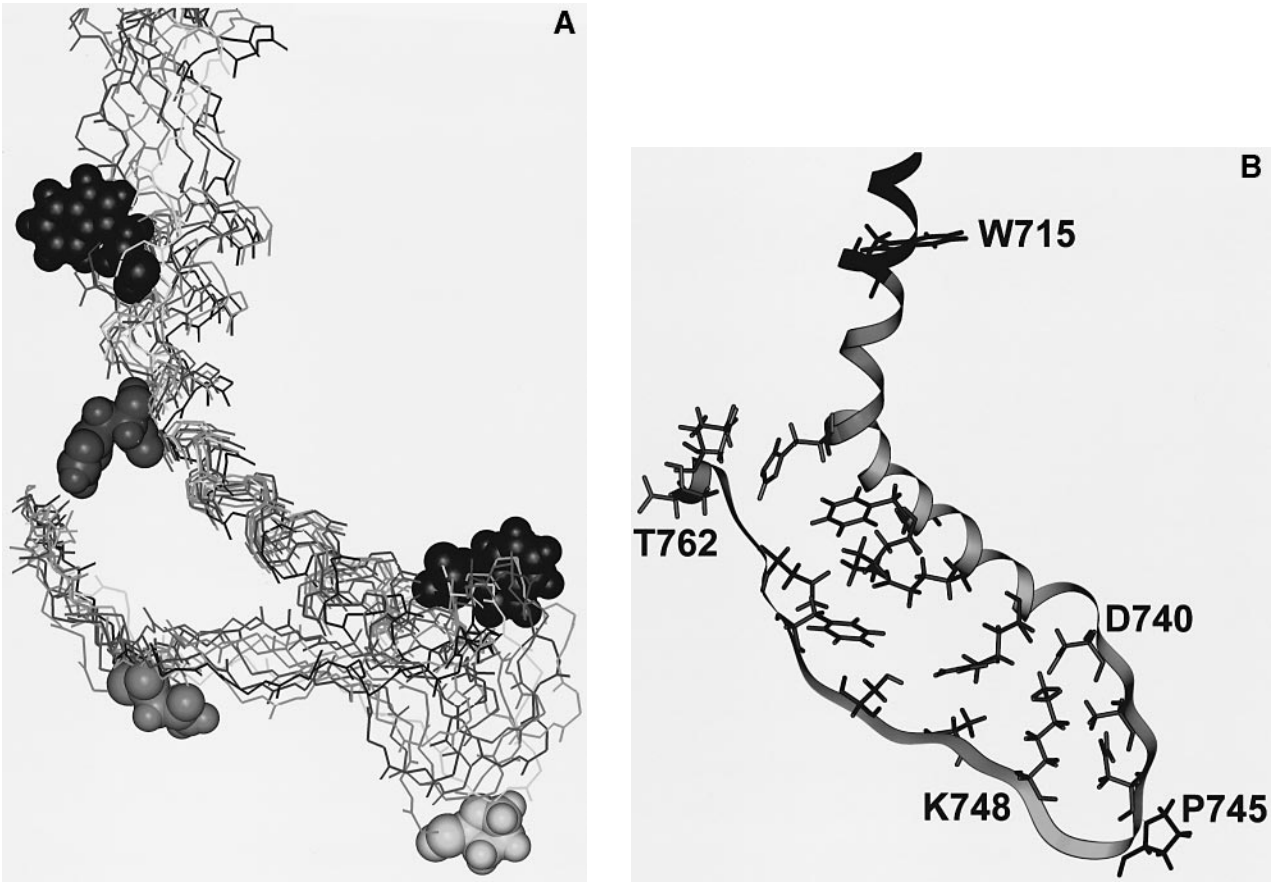

Fig. 7. Molecular dynamic models of β_3. The 10 energy minimized structures of model β_3, obtained during the molecular simulation procedure (**A**), and the final energy minimized structure of Model β_3 (**B**) are displayed. (A) For clarity, only the backbone of each structure of $\beta_3$701–1008 is displayed. For orientation, the side chain of tryptophans $\beta_3$715 and $\beta_3$739 (black spheres), histidine $\beta_3$722 (dark grey spheres), proline $\beta_3$745 (light grey spheres), and asparagine $\beta_3$756 (medium grey spheres) are displayed. (B) The backbone of $\beta_3$711–762 is displayed as a ribbon, and only a few side chains involved in inter-subunit contacts are displayed. The transmembrane portion of β_3, $\beta_3$711–715, and the side chain of tryptophan $\beta_3$715 and proline $\beta_3$745 are shaded black.

in the second model, model $\alpha_{IIb}\beta_3$Ca2, α_{IIb}995 was docked to $\beta_3$723. After docking, each cytoplasmic portion of the model was soaked with water, the energy of the assembly minimized, 50 ps of molecular dynamic simulations and 100 ps of the molecular simulation procedure was performed, followed by an energy minimization to a maximum derivative of less than 0.01 kcal·(mol·Å)$^{-1}$. The final structure for the two complex models are shown in Figure 8.

In both models, numerous contact sites (distances of $<$4.2 Å), both electrostatic and hydrophobic in nature, were observed between α_{IIb} and β_3. In the first complex model (model $\alpha_{IIb}\beta_3$Ca1), possible salt-bridges ($<$2.5 Å) between α_{IIb}1008 and $\beta_3$724, and between α_{IIb}996 and $\beta_3$734 were observed (Figure 8A). In the second complex model (Figure 8B), the salt bridge between α_{IIb}995 and $\beta_3$723 remained intact through the molecular dynamics/minimization procedure, and additional salt bridges between α_{IIb}1005 and $\beta_3$724 and between α_{IIb}1005 and $\beta_3$734 were predicted. A few major differences between the two models were noted. In model $\alpha_{IIb}\beta_3$Ca1, sites coordinating calcium binding were provided by amino acids from both α_{IIb} and β_3, while calcium remained coordinated only to α_{IIb} in model $\alpha_{IIb}\beta_3$Ca2. Most importantly, in model $\alpha_{IIb}\beta_3$Ca1, $\beta_3$716–721 and $\beta_3$741–754 formed α-helices. In contrast, in the second complex model, only a small α-helix ($\beta_3$729–732) was present, with $\beta_3$716–721 adopting either a turn ($\beta_3$716, 717 and 721) or a random coil ($\beta_3$718–720) conformation.

Discussion

In this study, we have developed structural models for both cytoplasmic tails of $\alpha_{IIb}\beta_3$, for calcium binding to the high affinity cation binding site in α_{IIb}, and for the α–β–cation cytoplasmic domain of $\alpha_{IIb}\beta_3$. These models have led us to predict the presence of specific structural elements within each cytoplasmic tail. Furthermore, examination of the conformation of the two cytoplasmic tails of $\alpha_{IIb}\beta_3$ alone and in complex has provided plausible explanations for the functional consequences of a number of the mutations introduced into the cytoplasmic tails.

In the final model for the cytoplasmic tail of α_{IIb}, the negatively charged C-terminus was found to fold back onto itself and to potentially interact with its positively charge N-terminus (Figure 3). The sites of intramolecular contact involved both side-chain and backbone interactions. These intra-subunit contacts may play a role in the stabilization of the conformations of α_{IIb}985–1008. The CD spectra of the α_{IIb} peptides also supports a model containing intra-subunit contacts. The CD spectrum for α_{IIb}985–998 displayed a high degree of β structure while α_{IIb}985–1008 displayed none (Figure 1), suggesting that contacts between α_{IIb}985–998 and α_{IIb}999–1008 suppressed the β structural potential of α_{IIb}985–1008 in favor of an α-helical arrangement. Furthermore, it should be noted that the CD spectra are consistent and correlate with our molecular models. For example, the CD spectra of

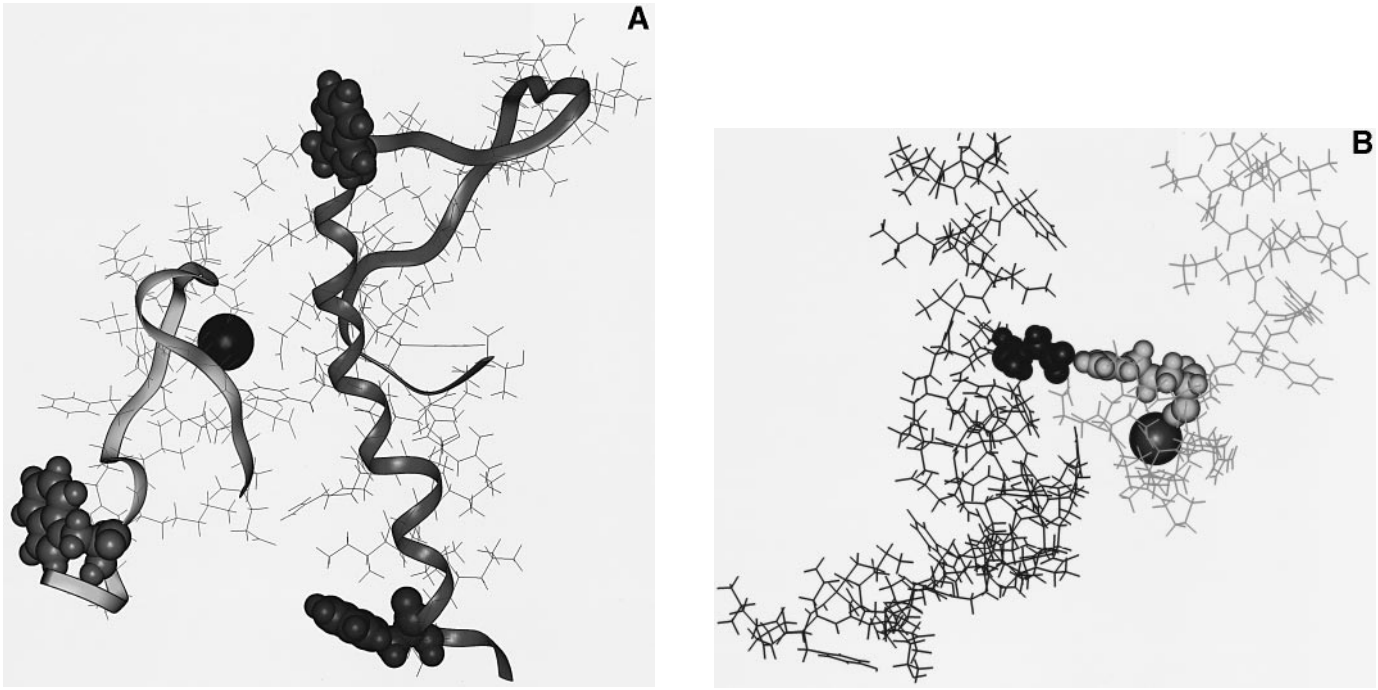

Fig. 8. Molecular models of the ternary cytoplasmic complex of $\alpha_{IIb}\beta_3$. (**A**) Proposed model fo the $\alpha_{IIb}\beta_3$ cytoplasmic complex as predicted in our previous study (Haas and Plow, 1996). The backbone of each subunit is highlighted with a ribbon and the calcium ion is displayed as a sphere. β_3 is displayed on the left (dark ribbon) and α_{IIb} on the right (light ribbon). The two tryptophans in β_3 (715 and 739) and the one in α_{IIb} (988) are displayed as spheres. (**B**) Proposed model of the $\alpha_{IIb}\beta_3$ cytoplasmic complex involving a salt bridge between α_{IIb}R995 and β_3D723 (Hughes *et al.*, 1996). β_3 (left structure) and α_{IIb} (right structure) are displayed as a dark and light sticks, respectively. The calcium ion is displayed as a large sphere, and $\beta_3$723 and α_{IIb}995 are highlighted as small dark and light spheres, respectively.

α_{IIb}999–1008 clearly demonstrated that the C-terminus of α_{IIb} does not adopt an α-helical, β-sheet or β-turn structure, consistent with all α_{IIb} models. Our CD data also identified that only a small portion of α_{IIb}985–999 can adopt an α-helical conformation, again consistent with the models. In the absence of other structural data, it was reassuring that the CD data correlated with the molecular models.

Using peptides corresponding to the entire cytoplasmic tails of α_{IIb} and β_3, we previously demonstrated that divalent cations (calcium, magnesium and manganese) bind to α_{IIb} (Haas and Plow, 1996). However, it is not known whether the cytoplasmic domain of $\alpha_{IIb}\beta_3$ binds cations *in situ* in platelets. In support of this possibility, we have shown that purified $\alpha_{IIb}\beta_3$ contains a high affinity cation binding site which could not be assigned to an extracellular site (Cierniewski *et al.*, 1994). *In situ* experiments are currently being conducted to test our peptide results. The cytoplasmic tail of α_{IIb} had similar affinities for calcium, magnesium and manganese (Haas and Plow, 1996). Which of these cations would bind to α_{IIb} *in situ* is not known. Our CD data demonstrates that the binding of cations to cytoplasmic α_{IIb} peptides does not cause a significant perturbation of conformation. Therefore, in developing cation–α_{IIb} models only one cation was modeled, calcium, as it is likely that the site could also accommodate other cations. Furthermore, in this study, as in our previous one (Haas and Plow, 1996), we used α_{IIb} with a free C-terminus, in accordance with the deduced amino acid sequence from the cDNA (Poncz *et al.*, 1987). Calvete *et al.* (1990) has provided evidence that the C-terminus of α_{IIb} is often an amide in platelets. Does amidation effect cation coordination and/or the structure of α_{IIb}? Amidation had no observed effect on the affinity of cations for α_{IIb}985–1008 (Haas and Plow, 1996), and the terminal carboxyl group provides only one cation coordination site in only one model (Table II). No differences between the CD spectra of α_{IIb} 985–1008 in its free acid or amide form were observed (data not shown), and the C-terminus of α_{IIb} did not coordinate with the β_3 cytoplasmic tail in the ternary cytoplasmic complex. Therefore, whether the C-terminus is an amide versus a free acid appears to be structurally silent.

In the docking of calcium to α_{IIb}999–1008, three models were generated (Figure 4). In all three models, the cation binding was found to be of high affinity, and its binding was coordinated by sites not only within α_{IIb}999–1008, but also by coordination sites within α_{IIb}985–998. Thus, cations are likely to enhance and/or stabilize the intra-subunit contacts between α_{IIb}985–998 and α_{IIb}000–1008, but are not essential for the interaction. In models of the ternary α_{IIb}–β_3–calcium cytoplasmic complex, additional cation coordination sites were provided by β_3, as well as numerous contacts sites between α_{IIb}999–1008 and β_3.

Besides α_{IIb}, the only other well-characterized α subunit known to associate with β_3 to form a functional integrin is α_v (Hynes, 1992). In comparing the sequences of the cytoplasmic tails of α_{IIb} and α_v (Table I), a few similarities were noted. Both α subunits retain the WKXGFFKR motif which is conserved amongst all α subunits. In addition, both α subunits contain a PP motif following the conserved region and both subunits contain a very acidic C-terminus, which, in combination, these two features distinguish α_{IIb} and α_v from all other α subunits. Thus, the structure of the α_v cytoplasmic tail is likely to be similar to that of α_{IIb} and may, therefore, function in a similar manner to that of α_{IIb}. Of the remaining α subunits, the cytoplasmic tail of α_2, α_3, α_4 and α_L appear to have potential for cation binding (Table I), but they lack the PP motif.

The structure of the cytoplasmic tail of β_3 is considerably more complex than that of α_{IIb}. In all models generated, the

NPXY motif at $\beta_3$744–747 was located at the vertex of β_3, and adopted either a turn or a loop conformation. Recently, tyrosine $\beta_3$747 has been reported to be a site of phosphorylation following receptor occupancy (Law *et al.*, 1996). Phosphorylation of the NPXY sequence resulted in the binding of SH2-containing adaptor proteins, including members of the Src family and/or Syk (Law *et al.*, 1996). Additional studies support the role for the phosphorylation of the NPXY as a prerequisite for the binding of the SH2-containing adaptor proteins (Prigent *et al.*, 1995). Thus, $\alpha_{IIb}\beta_3$ outside-in signaling may be mediated through a SH2-adaptor protein-coupled process. Following platelet activation, this NPXY region has also been implicated in cytoskeletal attachment (Reszka *et al.*, 1992; Otey *et al.*, 1993). In our models, this region of β_3 is surface accessible and it is not involved in α_{IIb} engagement, indicating that it should normally be accessible to tyrosine kinases, phosphatases and cytoskeletal elements. However, in unactivated platelets, at present it appears that the cytoplasmic domain of $\alpha_{IIb}\beta_3$ does not interact with these cellular proteins, and may be constituently occupied by an 'intracellular ligand'. β_3 endonexin (Shattil *et al.*, 1995) is a potential intracellular candidate.

In all models of β_3, a salt bridge is predicted to form between D740 and K748. This salt bridge may stabilize the NPLY turn-motif, but is probably not essential for formation of the β-turn; rather, it may be weak enough to be broken and allow for conformational changes to occur (Waldburger *et al.*, 1995). In the cytoplasmic domain of the epidermal growth factor receptor, a similar 'bridge regulation' model has been produced, in which a hydrogen-bond stabilizes an active region of the receptor (Timms *et al.*, 1995). If one compares all the β integrin sequences (partial listing in Table III), the potential salt bridge or hydrogen bonding pair is conserved: the residues corresponding to β_3K748 is either a lysine or arginine, and to β_3D740 is either an aspartate, asparagine, glutamine or glutamate. In one study of β_1 integrins, single point mutations of both residues were constructed. (Reszka *et al.*, 1992). Mutating either residue individually (β_1D781 and β_1K789), had little effect on localization of β_1 integrins to focal adhesions. It should be emphasized that the β_3D740–K748 salt bridge was predicted solely on the basis of molecular modeling. One problem with molecular modeling is that salt bridge and hydrophobic interactions can be over-emphasized. To minimize this problem, our models were developed in water to help shield the van der Waals and electrostatic attractive and repulsive forces of distal atoms from each other. Furthermore, we subjected our models to elevated temperatures, to inject enough energy into the system to break up these interactions. However, we did not include monovalent cations and anions (NaCl or KCl) into our models which might have reduced the probability of the β_3D740–K748 salt bridge from forming. Nevertheless, this salt bridge, as well as other intra-subunit interactions, were present in all β_3 models, provided theoretical support for their existence.

The α-helical content of $\beta_3$723–735 was also retained in all models, while considerable variation in the conformation of $\beta_3$713–720 and $\beta_3$750–762 were noted. Common to all β_3 models was the numerous contacts between the two halves of the cytoplasmic tail of β_3, divided at the NPXY motif. Some of the contacts are highlighted in the final model for β_3 (Figure 7B). In modeling a variant of β_3 (van Kuppevelt *et al.*, 1989), which deviates before the NPXY motif, these intra-subunit contact sites were lacking and the α-helix at $\beta_3$723–735 degenerated (data not shown). These data suggest that these intra-subunit contacts are required to stabilize the α-helical content of $\beta_3$723–735. It is therefore not surprising that mutation of the NPXY turn motif has dramatic functional consequences on the affinity states of $\alpha_{IIb}\beta_3$ (O'Toole *et al.*, 1995).

In docking of the two cytoplasmic models together to form a structural model for the cytoplasmic domain of $\alpha_{IIb}\beta_3$, there are a number of possible docking sites. Predicated on our previous study (Haas and Plow, 1996), we docked α_{IIb}999–1008 to the 'cyto 1' region in β_3. The second model was based upon the formation of a salt bridge between α_{IIb}R995 and β_3D723 (Hughes *et al.*, 1996). The most striking difference between these two models is the conformation adopted by the juxta-transmembrane region in β_3, $\beta_3$716–721. In the first model, this region assumes an α-helix, while in the second model it adopts both a turn and a random coil conformation. Overall, these differences indicate that $\beta_3$716–721 is conformationally labile, in agreement with our CD data. Given that the juxta-transmembrane region is ideally located to regulate integrin signaling, both inside-out and outside-in, we propose that the key structural component of integrin signaling is the switching in conformation which the juxta-transmembrane region undergoes. Thus, the α/β (and β/β) contact sites which stabilize one conformation over the other are central to integrin function. It is very likely that the interaction of some cytosolic proteins with the cytoplasmic domain of $\alpha_{IIb}\beta_3$ will alter these α/β contact sites, and in doing so, will lead to the stabilization of one conformation over the other. This may well be an underlying mechanism of integrin signaling. These cytosolic proteins may be the ones interacting with the NPXY motif (discussed above), or may be ones which interfere directly with the α/β contact sites. Moreover, because of the NPXY turn, the C-terminus of β_3 resides in close proximity to the juxta-transmembrane region. Thus, any cellular protein which interacts with this C-terminal region, could possibly influence the conformation of the β_3 juxta-transmembrane region. Such may be the case for β_3-endonexin (Shattil *et al.*, 1995).

Our models predict multiple contacts between α_{IIb} and β_3 involving α_{IIb} residues within the highly conserved GFFKR motif and within its acidic tail. In agreement, truncation of α_{IIb} after V991, immediately before the GFFKR motif, causes a major change in the function of $\alpha_{IIb}\beta_3$, leading to a constitutively active receptor, which is not suppressed by addition of the cytoplasmic tail of α_2, α_5 or $\alpha_{6A/B}$ (O'Toole *et al.*, 1991 and 1994). As the GFFKR motif is conserved in α_5, these data suggest that residues distal to this GFFKR motif (the acid tail of α_{IIb}) must be important in regulating inside-out signaling. However, truncation of the segments distal to the GFFKR motif results in receptors which reside in a low affinity states in α_{IIb}, α_4 and α_5 (Huttenlocher *et al.*, 1996; Kassner and Hemler, 1993; Sarita *et al.*, 1996). Deletion of the GFFKR motif in a α_{IIb}/α_L chimera places the receptor into a high affinity state (O'Toole *et al.*, 1994; Huttenlocher *et al.*, 1996; Peter and Bode, 1996). Single point alanine substitutions of all residues but the lysine in the GFFKR motif also places $\alpha_{IIb}\beta_3$ in a high affinity state (Hughes *et al.*, 1996). These data suggest that residues in both the amino and carboxyl region of the cytoplasmic domain of α_{IIb} are required for normal inside-out signaling by $\alpha_{IIb}\beta_3$. The GFFKR motif which is correctly positioned in parallel with the conformationally labile juxta-transmembrane region of β_3, $\beta_3$716–721, may be critical for maintaining $\alpha_{IIb}\beta_3$ in a low affinity state, possibly by

controlling the conformation of $\beta_3$716–721. The cation binding properties of the acidic terminus of $\alpha_{IIb}\beta_3$ may also be important as it can not be replaced with that of α_5 which is unlikely to bind cation, but can be replaced with that of α_L, which possibly could (O'Toole *et al.*, 1991. Loh *et al.*, 1995; Huttenlocher *et al.*, 1996). Compounding the interpretation of mutational studies is that alterations in $\alpha_{IIb}\beta_3$ function by various mutations is cell dependent (O'Toole *et al.*, 1994; Loh *et al.*, 1996). High resolution NMR or crystal structure of the transmembrane/cytoplasmic domain of $\alpha_{IIb}\beta_3$, followed by detailed mutational analysis of structurally important residues in a number of cellular environments, may ultimately be necessary to resolve these highly complex relationships.

Acknowledgements

This work was supported by National Institutes of Health Grants HL54924. Dr Haas was supported by a fellowship from the American Heart Association, Northeast Ohio Affiliate.

References

Backer,J.M., Shoelson,S.E., Weiss,M.A., Hua,Q.X., Cheatham,R.B., Haring,E., Cahill,D.C. and White,M.F. (1992) *J. Cell Biol.*, **118**, 831–839.

Bansal,A. and Gierasch,L.M. (1991) *Cell*, **67**, 1195–1201.

Bjornholm,B., Jorgensen,F.S. and Schwartz,T.W. (1993) *Biochemistry*, **32**, 2954–2959.

Buck,M., Radford,S.E. and Dobson,C.M. (1993) *Biochemistry*, **32**, 669–678.

Calvete,J.J., Schafer,W., Henschen,A. and Gonźalez-Rodriguez,J. (1990) *FEBS Lett.*, **263**, 43–46.

Cappolino,M., Leung-Hagesteijn,C., Dedhar,S. and Wilkins,J. (1995) *J. Biol. Chem.*, **270**, 23132–23138.

Chen,Y.-P., Djaffar,I., Pidard,D., Steiner,B., Cieutat,A.-M., Caen,J.P. and Rosa,J.-P. (1992) *Proc. Natl Acad. Sci. USA*, **9**, 10169–10173.

Chen,Y.-P., O'Toole,T.E., Yl̈anne,J., Rosa,J.-P. and Ginsberg,M.H. (1994) *Blood*, **84**, 1847–1865.

Chuang,C.C., Huang,W.C., Yu,H.M., Wang,K.T. and Wu,S.H. (1996) *Biochim. Biophys. Acta Protein Struct. Mol. Enzymol.*, **1291**, 1–8.

Clark,E.S., Shattil,S.J. and Brugge,J.S. (1994) *Trends Biochem. Sci.*, **19**, 464–469.

Clark,E.A. and Brugge,J.S. (1995) *Science*, **268**, 233–239.

Fitzgerald,L.A., Steiner,B., Rall,S.C.,Jr., Lo,S.-S. and Phillips,D.R. (1987) *J. Biol. Chem.*, **262**, 3936–3939.

Fornaro,M., Zheng,D.Q. and Languini,L.R. (1995) *J. Biol. Chem.*, **270**, 24666–2l4669.

Fox,J.E.B. (1993) *Thromb. Haemost.*, **70**, 884–893.

Ginsberg,M.H., Du,X. and Plow,E.F. (1992) *Curr. Opin. Cell Biol.*, **4**, 766–771.

Ginsberg,M.H., Xiaoping,D., O'Toole,T.E., Loftus,J.C. and Plow,E.F. (1993) *Thromb. Haemost.*, **70**, 87–93.

Haas,T.A. and Plow,E.F. (1994) *Curr. Opin. Cell Biol.*, **6**, 656–662.

Haas,T.A. and Plow,E.F. (1996) *J. Biol. Chem.*, **271**, 6017–6026.

Horwitz,A., Duggan,K., Buck,C., Beckerle,M.C. and Burridge,K. (1986) *Nature*, **320**, 531–533.

Hughes,P.E., O'Toole,T.E., Yl̈anne,J., Shattil,S.J. and Ginsberg,M.H. (1995) *J. Biol. Chem.*, **270**, 12411–12417.

Hughes,P.E., Diaz-Gonzalez,F., Leong,L., Wu,C., McDonald,J.A., Shattil,S.J. and Ginsberg,M.H. (1996) *J. Biol. Chem.*, **271**, 6571–6574.

Huttenlocher,A., Ginsberg,M.H. and Horwitz,A.F. (1996) *J. Cell Biol.*, **134**, 1551–1562.

Hynes,R.O. (1992) *Cell*, **69**, 11–25.

Kassner,P.D. and Hemler,M.E. (1993) *J. Exp. Med.*, **178**, 649–660.

Kieffer,J.D., Plopper,G., Ingber,D.E., Hartwig,J.H. and Kupper,T.S. (1995) *Biochim. Biophys. Res. Commun.*, **217**, 466–474.

Law,D.A., Nannizzi-Alaimo,L. and Phillips,D.R. (1996) *J. Biol. Chem.*, **271**, 10811–10815.

Loftus,J.C., Smith,J.W. and Ginsberg,M.H. (1994) *J. Biol. Chem.*, **269**, 25235–25238.

Loh,E., Beaverson,K., Vilaire,G., Qi,W., Poncz,M. and Bennett,J.S. (1995) *J. Biol. Chem.*, **270**, 18631–18636.

Loh,E., Qi,W., Vilaire,G. and Bennett,J.S. (1996) *J. Biol. Chem.*, **271**, 30233–30241.

Lyu,P.C., Zhou,H.X., Jelveh,N., Wemmer,D.E. and Kallenbach,N.R. (1992) *J. Am. Chem. Soc.*, **114**, 6560–6562.

Lyu,P.C. and Wemmer,D.E. (1993) *Biochemistry*, **32**, 421–425.

Marcantonio,E.E., Guan,J.-L., Trevithick,J.E. and Hynes,R.O. (1990) *Cell Regul.*, **1**, 597–604.

Meredith,J., Takada,Y., Fornaro,M., Languino,L.R. and Schwartz,M.A. (1995) *Science*, **269**, 1570–1572.

O'Toole,T.E., Mandelman,D., Forsyth,J., Shattil,S.J., Plow,E.F. and Ginsberg,M.H. (1991) *Science*, **254**, 845–847.

O'Toole,T.E., Katagiri,Y., Faull,R.J., Peter,K., Tamura,R., Quaranta,V., Loftus,J.C., Shattil,S.J. and Ginsberg,M.H. (1994) *J. Cell Biol.*, **124**, 1047–1059.

O'Toole,T.E., Ylanne,J. and Culley,B.M. (1995) *J. Biol. Chem.*, **270**, 8553–8558.

Otey,C.A., Vasquez,G.B., Burridge,K. and Erickson,B.W. (1993) *J. Biol. Chem.*, **268**, 21193–21197.

Peter,K. and Bode,C. (1996) *Blood Coag. Fibrinol.*, **7**, 233–236.

Ponz,M., Eisman,R., Heidenreich,R., Silver,S.M., Vilaire,G., Surrey,S., Schwartz,E. and Bennett,J.S. (1987) *J. Biol. Chem.*, **262**, 8476–8482.

Prigent,S.A., Pillay,T.S., Ravichandran,K.S. and Gullick,W.J. (1995) *J. Biol. Chem.*, **270**, 22097–22100.

Reszka,A.A., Hayashi,Y. and Horwitz,A.F. (1992) *J. Cell Biol.*, **117**, 1321–1330.

Riek,R.P., Handshumacher,M.D., Sung,S.-S., Tan,M., Glynias,M.J., Schulchter,M.D., Novotny,J. and Graham,R.M. (1995) *J. Theor. Biol.*, **172**, 245–258.

Rojiani,M.V., Finlay,B.B., Gray,V. and Dedhar,S. (1993) *Biochemistry*, **30**, 9859–9866.

Ruoslahti,E. (1991) *J. Clin. Invest.*, **87**, 1–5.

Sarita,K.S., Lakonishok,M., Thomas,D.A., Muschler,J. and Horwitz,A.F. (1996) *J. Cell Biol.*, **133**, 169–184.

Schnolzer,M., Alewood,P., Jones,A., Alewood,D. and Kent,S.B. (1993) *Int. J. Pept. Protein Res.*, **40**, 180–193.

Schwartz,M.A. (1992) *Trends Cell Biol.*, **2**, 304–308.

Shattil,S.J., O'Toole,T.E., Eigenthaler,M., Thon,V., Williams,M., Babior,B.M. and Ginsberg,M.H. (1995) *J. Cell Biol.*, **131**, 807–816.

Sticht,H., Willbold,D., Ejchart,A., Rosin-Arbesfeld,R., Yaniv,A., Gazit,A. and Rösch,P. (1994) *Eur. J. Biochem.*, **225**, 855–861.

Timms,J.F., Noble,M.E.M. and Gregoriou,M. (1995) *Biochem. J.*, **308**, 219–229.

Tuckwell,D.S., Brass,A. and Humphries,M.J. (1993) *Biochem. J.*, **285**, 325–331.

van Kuppevelt,T.H., Languino,L.R., Gailit,J.O., Suzuki,S. and Ruoslahti,E. (1989) *Proc. Natl Acad. Sci. USA*, **86**, 5415–5418.

Waldburger,C.D., Schildbach,J.F. and Sauer,R.T. (1995) *Nat. Struct. Biol.*, **2**, 122–128.

Yang,J.J., Pitkeathly,M. and Radford,S.E. (1994) *Biochemistry*, **33**, 7345–7353.

Zhang,J., Fry,M.J., Waterfield,M.D., Jaken,S., Liao,L., Fox,J.E.B. and Rittenhouse,S.E. (1992) *J. Biol. Chem.*, **267**, 4686–4692.

Received May 8, 1997; revised July 30, 1997; accepted September 5, 1997